2012

Estimating seasonal evapotranspiration from temporal satellite images

Ramesh K. Singh
USGS EROS Center, Sioux Falls, SD, rsingh@usgs.gov

Shuguang Liu
U.S. Geological Survey, EROS, sliu@usgs.gov

Larry L. Tieszen
USGS EROS, tieszen@usgs.gov

Andrew E. Suyker
University of Nebraska-Lincoln, asuyker1@unl.edu

Shashi B. Verma
University of Nebraska-Lincoln, sverma1@unl.edu

Irrig Sci (2012) 30:303–313
DOI 10.1007/s00271-011-0287-z

ORIGINAL PAPER

Estimating seasonal evapotranspiration from temporal satellite images

Ramesh K. Singh · Shuguang Liu · Larry L. Tieszen · Andrew E. Suyker · Shashi B. Verma

Received: 17 June 2010 / Accepted: 15 April 2011 / Published online: 30 April 2011

Abstract Estimating seasonal evapotranspiration (ET) has many applications in water resources planning and management, including hydrological and ecological modeling. Availability of satellite remote sensing images is limited due to repeat cycle of satellite or cloud cover. This study was conducted to determine the suitability of different methods namely cubic spline, fixed, and linear for estimating seasonal ET from temporal remotely sensed images. Mapping Evapotranspiration at high Resolution with Internalized Calibration (METRIC) model in conjunction with the wet METRIC (wMETRIC), a modified version of the METRIC model, was used to estimate ET on the days of satellite overpass using eight Landsat images during the 2001 crop growing season in Midwest USA. The model-estimated daily ET was in good agreement ($R^2 = 0.91$) with the eddy covariance tower-measured daily ET. The standard error of daily ET was 0.6 mm (20%) at three validation sites in Nebraska, USA. There was no statistically significant difference ($P > 0.05$) among the cubic spline, fixed, and linear methods for computing seasonal (July–December) ET from temporal ET estimates. Overall, the cubic spline resulted in the lowest standard error of 6 mm (1.67%) for seasonal ET. However, further testing of this method for multiple years is necessary to determine its suitability.

Communicated by S. Ortega-Farias.

R. K. Singh (✉)
ASRC Research and Technology Solutions at US Geological Survey (USGS) Earth Resources Observation and Science (EROS) Center, 47914 252nd Street, Sioux Falls, SD 57198, USA
e-mail: rsingh@usgs.gov

S. Liu · L. L. Tieszen
USGS EROS, Sioux Falls, SD 57198, USA

A. E. Suyker · S. B. Verma
School of Natural Resources, University of Nebraska-Lincoln, Lincoln, NE 68583, USA

Introduction

A spatially explicit and quantitative understanding of evapotranspiration (ET) is critical for planning and managing water resources. It also helps in developing a better understanding of the soil–plant–atmosphere interactions, carbon fluxes, nutrient biogeochemistry, and climatic variability due to strong coupling between carbon and ET (Nemani et al. 2002; Beer et al. 2007; Suyker and Verma 2010). However, it is challenging to upscale point measurements of ET to regional scales, especially for different land use/land cover under diverse management practices. Remote sensing techniques have emerged as a very useful tool for estimating ET at various temporal and spatial scales. In recent years, the energy balance approach is increasingly used for quantifying ET using remotely sensed data (Gowda et al. 2008). Remote sensing-based energy balance methods provide instantaneous ET estimates. As the instantaneous ET values are of less practical use, these values are converted to daily ET using different methods such as evaporative fraction (Shuttleworth et al. 1989; Brutseart and Sugita 1992), and alfalfa referenced ET fraction (ET_rF) (Trezza 2002). Shuttleworth et al. (1989) showed that the evaporative fraction for homogeneous surfaces remains nearly constant during the daytime. Chavez et al. (2008a) compared six different methods for extrapolating the instantaneous ET to daily ET using airborne remote sensing data from Iowa for maize and soybean crops. The evaporative fraction method worked better for water-stressed crops under non-advective and heterogeneous vegetation cover conditions; whereas the

ET_rF method performed better for crops under conditions of non-stress moisture, advective, and homogeneous surface (Chavez et al. 2008a). While comparing with lysimeter data, Allen et al. (2007a) found that ET_rF-based daily ET was in better agreement with actual values than evaporative fraction-based daily ET, for advective conditions.

Many applications in water resources planning and management require seasonal/annual ET estimates. The computation of remote sensing-based seasonal/annual ET is very challenging when daily ET is not available due to temporal resolution of satellites and/or gaps in image acquisition due to cloud cover. Although there are different methods of extrapolating instantaneous ET to daily ET (Chavez et al. 2008a), methods for interpolating/extrapolating daily ET to seasonal/annual ET are limited. Bastiaanssen et al. (2002) used the Surface Energy Balance Algorithm for Land (SEBAL model, Bastiaanssen et al. 1998a, b) for annual ET estimation across the Indus Basin and reported that annual ET varied from 0 to 10% on field scale and to 5% at the regional scale when compared to a field-scale transient moisture flow model (Soil Water Atmosphere Plant, SWAP model), in situ Bowen ratio measurements, and residual water balance analysis. Allen et al. (2007a) used the accumulated alfalfa referenced ET (ET_r) and the ET_rF for the image date for computing seasonal ET. This approach resulted in less than 1% difference between the Mapping Evapotranspiration at high Resolution with Internalized Calibration (METRIC model, Allen et al. 2007a, b) estimated seasonal ET (714 mm) and lysimeter measured seasonal ET (718 mm) for the sugar beet crop. They attributed this remarkably good estimation of seasonal ET to the random distribution of daily ET from the METRIC model. Chavez et al. (2008b) used a grass-referenced ET fraction (ET_oF) with cumulative grass reference ET for estimating cumulative/seasonal ET. They reported that the mean bias error and root mean square error of cumulative ET for 2-month period were −8.9 mm (−3.6%) and 30.4 mm (12.5%), respectively. Allen et al. 2007c also suggested linear and cubic spline interpolations of ET_rF between the processed image dates and multiplying these values with daily ET_r for a seasonal ET estimation.

Our objective of this study was to evaluate three different methods namely cubic spline, fixed ET_rF, and linear methods for estimating seasonal ET from temporal Landsat satellite images.

Materials and methods

Satellite and field data

This study was conducted using four Thematic Mapper (TM) images acquired on July 4, August 5, October 24, December 11, and four Enhanced Thematic Mapper Plus (ETM+) images acquired on August 13, August 29, September 30, and October 16 during 2001 crop growing season from Midwest USA (Fig. 1). The TM sensor onboard Landsat 5 has seven spectral bands—six bands with 30-m spatial resolution in the shortwave, near infrared, and mid-infrared portions of the electromagnetic spectrum while another band, the thermal band, has a pixel spatial resolution of 120 m. The ETM+ onboard Landsat 7 has eight spectral bands—six bands with 30-m spatial resolution in the shortwave, near infrared, and mid-infrared portions of the electromagnetic spectrum while another band, the thermal band, has a pixel spatial resolution of 60 m. The panchromatic band in ETM + with 15-m spatial resolution was not used in this study. The METRIC model (Allen et al. 2007b, c) in conjunction with the wet METRIC (wMETRIC) model (Singh 2009; Singh and Irmak 2011) was used for estimating ET using the remotely sensed images. The wMETRIC model procedure was followed for images having higher residual moisture content at the hot pixel (Alfalfa referenced ET fraction (ET_rF) >0.15). Based on this criterion, the METRIC model was used for the images acquired on August 5, August 13, and September 30, while the wMETRIC model was applied for the rest of the images. In the wMETRIC model, the latent heat flux at the hot and cold pixels is computed using Priestley–Taylor method (Priestley and Taylor 1972). The model maker tool in Erdas Imagine® 9.3 image processing software (ERDAS Inc., Atlanta, Georgia) was used for coding the models' algorithms. The model-estimated ET accuracy was evaluated by comparing the average of 25 (5 × 5) pixels ET centered at the research field (Eddy

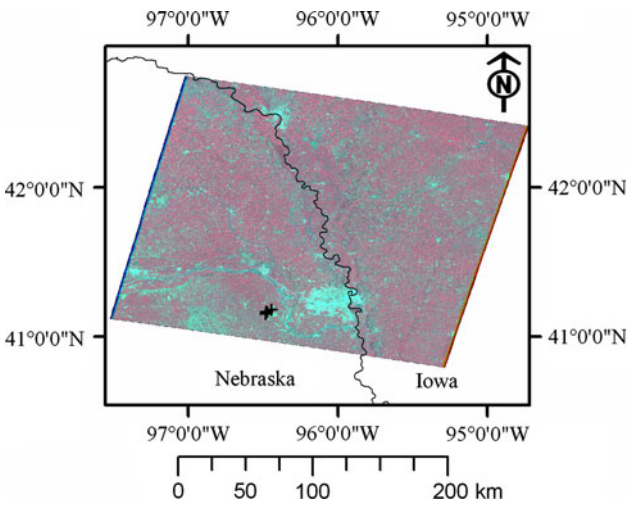

Fig. 1 False *Color* Composite (*Bands* 4, 3, 2) of the study area (Landsat, path 28, row 31). The Missouri River flows from *northwest* corner of the image to *southeast* corner bordering between Nebraska and Iowa states in USA. Location of the eddy covariance flux towers is also shown using *plus* (+) *symbols* within the image

Covariance (EC) tower) locations (Fig. 1). Although many studies (Twine et al. 2000; Wilson et al. 2002; Hollinger and Richardson 2005) have reported the systematic and random errors associated with the flux tower measurements, our emphasis here is on the comparison of three methods for estimating seasonal ET from temporal Landsat satellite images.

The field measurements of ET were obtained using the eddy covariance technique at the University of Nebraska Agricultural Research and Development Center (ARDC) near Mead, Nebraska, located about 64 km north of Lincoln, Nebraska. The general weather condition at the study site during 2001 is shown in Fig. 2. Mean monthly air temperature was below 0°C during December–February while the maximum precipitation occurred in May (Fig. 2a). Mean monthly wind speed during 2001 was 3.45 ± 0.82 m/s. The experimental sites at Mead are under no-till soil management with three different cropping systems: center-pivot irrigated continuous maize (site 1) (41°9′ 54.2″N, 96°28′ 35.9″W, 361 m above mean sea level, 48.7 ha), center-pivot irrigated maize–soybean rotation (site 2) (41°9′ 53.5″N, 96°28′ 12.3″W, 362 m above mean sea level, 52.4 ha), and rainfed maize–soybean rotation (site 3) (41°10′ 46.8″N, 96°26′ 22.7″W, 362 m above mean sea level, 65.4 ha). Maize was planted at these three sites during 2001 crop growing season (Table 1). The soils at these sites are mainly silty clay loams consisting of four soil series: Yutan (Fine-silty, mixed, superactive, mesic Mollic Hapludalfs), Tomek (Fine, smectitic, mesic Pachic Argiudolls), Filbert (Fine, smectitic, mesic Vertic Argialbolls), and Fillmore (Fine, smectitic, mesic Vertic Argialbolls), which are commonly found in the area. The general particle size distribution is 13% sand, 57% silt, 27.5% clay, and 2.5% organic matter with a volumetric soil water content level at field capacity of 0.32 m^3 m^{-3} and at permanent wilting point of 0.19 m^3 m^{-3}. The fluxes were measured using a three-dimensional sonic anemometer (Model R3, Gill Instruments Ltd., Lymington, UK) and an open-path infrared gas analyzing system (Model LI7500, Li-Cor Inc., Lincoln, Nebraska, US). The measured fluxes were corrected for inadequate sensor frequency response (e.g., Moore 1986) and variation in air density due to transfer of water vapor and sensible heat (e.g. Webb et al. 1980). Additional details about the sites, installation, operation and maintenance of EC tower, data processing, and quality control are available in previous publications (Verma et al. 2005; Suyker and Verma 2008, 2009).

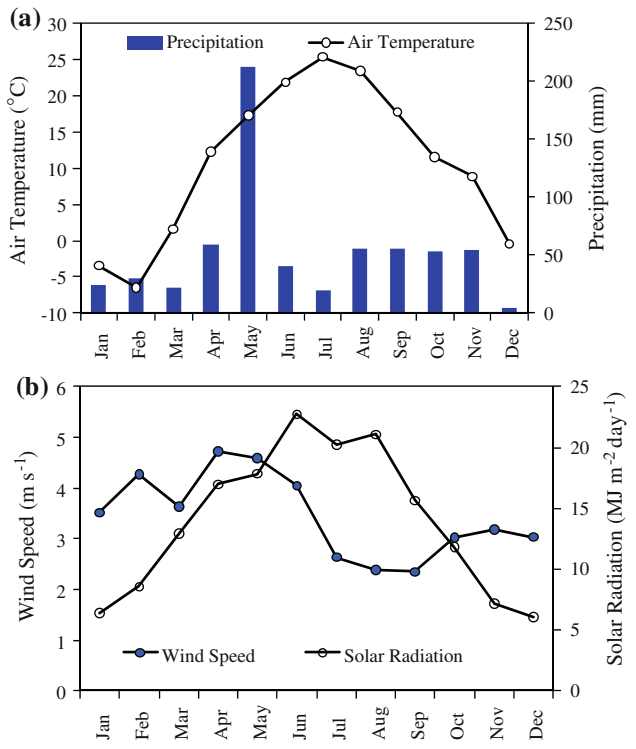

Fig. 2 General climate condition during 2001, at the study site measured at a nearby station Mead, Nebraska, showing (**a**) monthly mean air temperature and accumulated monthly precipitation, (**b**) monthly mean wind speed and monthly mean solar radiation

Estimation of ET_rF between days of satellite acquisitions

Three different methods of ET_rF estimation were used for computing seasonal ET in this study. Firstly, a fixed ET_rF based on representative image date was used for computing the ET_rF on the days between the acquired images. The ET_rF for any date was taken the same as ET_rF on the nearest dates of eight satellite image acquisitions. It was hypothesized that ET_rF on each acquired image date was constant during the representative period for daily ET computation. This method is simple to implement using any programming language. This method works well if the ET on image date is representative of that period. Second method of estimating ET_rF involved linear interpolation. For linear method, ET_rF was linearly interpolated between the two image acquisition dates. The errors caused by over- and underestimation of daily ET are canceled out while computing seasonal ET. The slope of the line at the image dates (i.e. knots) is discontinuous in the linear interpolation. This method is suitable if satellite images are available at regular interval and model estimates capture the pattern of the ET variation. The third interpolation method used was a cubic spline. The advantage of cubic spline is that the slope and curvature are continuous at the knots (Gerald and Wheatley 2004). For a cubic spline, at least 4 images are required. The cubic polynomial, $g_i(x)$, in the ith interval between two points (x_i, y_i), (x_{i+1}, y_{i+1}) can be written in the form:

Table 1 Cropping details at Agricultural Research and Development Center near Mead, Nebraska

Site	Crop: cultivar	Plant population (plants ha^{-1})	Planting date	Harvest date
Site 1	Maize: pioneer 33P67	82,000	May 10	October 18
Site 2	Maize: pioneer 33P67	81,000	May 11	October 22
Site 3	Maize: pioneer 33B51	53,000	May 14	October 29

$$g_i(x) = a_i(x - x_i)^3 + b_i(x - x_i)^2 + c_i(x - x_i) + d_i \quad (1)$$

The solution of cubic polynomial (Eq. 1) for spline conditions results in coefficients a_i, b_i, c_i, and d_i as given below:

$$a_i = \frac{S_{i+1} - S_i}{6h_i} \quad (2)$$

$$b_i = \frac{S_i}{2} \quad (3)$$

$$c_i = \frac{y_{i+1} - y_i}{h_i} - \frac{2h_iS_i + h_iS_{i+1}}{6} \quad (4)$$

$$d_i = y_i \quad (5)$$

where S_i is the second derivative of the cubic polynomial i.e. $S_i = g''(x_i)$, h_i is the width of the ith interval, i.e. $h_i = (x_{i+1} - x_i)$ for all $i = 0, 1, 2, \ldots$. The assumption of the natural spline for the end conditions of cubic spline resulted in $S_0 = S_3 = 0$. The remaining S_1 and S_2 were solved in matrix form as follows:

$$\begin{bmatrix} 2(h_0 + h_1) & h_1 \\ h_1 & 2(h_1 + h2_1) \end{bmatrix} \begin{bmatrix} S_1 \\ S_2 \end{bmatrix} = 6 \begin{bmatrix} f[x_1, x_2] - f[x_0, x_1] \\ f[x_2, x_3] - f[x_1, x_2] \end{bmatrix} \quad (6)$$

where $f\,[x_i, x_{i+1}]$ is the divided difference between x_i and x_{i+1} given as

$$f[x_i, x_{i+1}] = \frac{y_{i+1} - y_i}{x_{i+1} - x_i} \quad (7)$$

Thus, cubic spline for each interval was obtained using the above procedure based on four nearest image dates. All the three methods of ET_rF estimation were coded in Erdas Imagine using the model maker tool.

Monthly and seasonal evapotranspiration

Hourly and daily ET_r were computed using hourly meteorological data from the Mead, Nebraska, collected by the High Plains Regional Climate Center, University of Nebraska, Lincoln. The ASCE-EWRI (2005) procedure was followed for computing hourly ET_r using the hourly meteorological data and summed over 24 h to get daily ET_r. The daily ET for a particular date was computed by multiplying the representative ET_rF with the corresponding ET_r value, i.e.

$$ET = ET_rF \times ET_r \quad (8)$$

Daily computed ET values were summed on monthly basis to get the monthly ET, and monthly ET was added together to get the seasonal value. The performance of the daily, monthly, and seasonal ET was evaluated based on coefficient of determination (R^2), relative predictive error (PE), and standard error (SE) as:

$$R^2 = \frac{\left(\sum_{i=1}^{n}(O_i - \overline{O})(P_i - \overline{P})\right)^2}{\sum_{i=1}^{n}(O_i - \overline{O})^2 \sum_{i=1}^{n}(P_i - \overline{P})^2} \quad (9)$$

$$PE = \frac{(\overline{P} - \overline{O})}{\overline{O}} \times 100 \quad (10)$$

$$SE = \left[\frac{1}{(n-2)}\left(\sum_{i=1}^{n}(P_i - \overline{P})^2 - \frac{\left(\sum_{i=1}^{n}(O_i - \overline{O})(P_i - \overline{P})\right)^2}{\sum_{i=1}^{n}(O_i - \overline{O})^2}\right)\right]^{1/2} \quad (11)$$

where O_i and P_i are ith measured and estimated values, respectively, n is the number of observations, and $\overline{P}$ and $\overline{O}$ are the average estimated and measured values, respectively.

Results and discussion

Estimated and measured instantaneous fluxes

The estimated energy fluxes compared reasonably with the measured energy fluxes at the time of satellite overpass (Fig. 3). The estimated R_n was within 10% of the measured value with high R^2 (Table 2), indicating good ability of the model to estimate this energy component. The G component of the energy balance is relatively small in magnitude but difficult to estimate through modeling approaches due to changes in thermal conductivity and volumetric heat capacity of soil with varying moisture and vegetation. Our result showed that the predictive error of G was about −12% and only about 1/3 of the variability could be explained by the model (Table 2) in absent of any local calibration. The H was estimated reasonably at site 1 and site 2 when compared to estimation at site 3. Overall, there was good correlation between estimated and measured LE at all three sites, and the predictive error was just 2% with a standard error of 58 W m^{-2}.

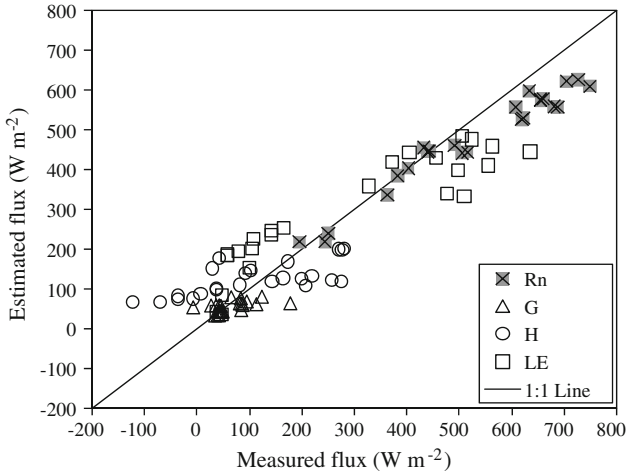

Fig. 3 Comparison of model-estimated and eddy covariance tower-measured instantaneous energy fluxes, namely net radiation (R_n), soil heat flux (G), sensible heat flux (H), and latent heat flux (LE) at the study sites

Table 2 Statistical details of comparison of measured and model-estimated instantaneous energy fluxes namely net radiation (R_n), soil heat flux (G), sensible heat flux (H), and latent heat flux (LE) at the study sites

		Predictive error (%)	Standard error (W m^{-2})	R^2 (−)
Site 1	R_n	−12.0	22	0.98
	G	16.5	15	0.03
	H	48.3	25	0.73
	LE	−4.0	61	0.88
Site 2	R_n	−11.4	30	0.96
	G	−6.6	12	0.36
	H	15.2	25	0.71
	LE	11.6	60	0.87
Site 3	R_n	−6.3	24	0.97
	G	−30.3	12	0.33
	H	−2.4	37	0.03
	LE	−0.4	55	0.80
Overall	R_n	−9.9	27	0.95
	G	−12.4	12	0.29
	H	14.8	30	0.50
	LE	−2.0	58	0.84

Accuracy of daily evapotranspiration estimation

Evapotranspiration in the METRIC and the wMETRIC models is the residual energy used for ET processes. Accuracy of the ET maps created from the Landsat images was carried out by pixels sampling and comparing with the EC tower measurement (Fig. 4). In general, the model-estimated ET followed the trend of EC tower-measured ET at all three sites. Overall, model estimates were higher on average by 22% as compared to the EC tower measurements. Suyker and Verma (2009, 2010) reported the mean and standard deviation of regression slopes between sum of net radiation (R_n) and soil heat flux (G) and sum of sensible heat (H) and latent heat (LE) fluxes (i.e., closure) for all sites/years to be 0.88 ± 0.04. In view of the difficulties associated with accurately estimating the canopy and mulch storage and other relevant terms (photosynthesis), "energy balance closure" at these study sites was considered reasonable, and our model versus measurement comparison seems acceptable. Twine et al. 2000 found that eddy covariance systems tend to underestimate the vapor fluxes with 10–30% systematic closure problem. Both site 1 and site 3 had good agreement on 5th August; however, discrepancy between measured and modeled ET at site 2 on this date is clearly evident. This was due to the fact that irrigation pivot passed over site 2 on 5th August, which affected the water flux measurements. Though the crop at all three sites was maize, the measured ET at site 2 (4.6 mm day^{-1}) was less than measured ET at dryland site 3 (5.1 mm day^{-1}) on 5th August, indicating underreporting. It should be noted that all three sites are located close to each other (within 1.6 km). The best agreement between EC tower and model ET was observed at site 1 ($R^2 = 0.93$) as compared to site 2 and site 3 (Table 3). Overall, about 90% variability was explained by the model estimate at these sites. In general, relative predictive error ranged from 17.7% (site 1) to 30% (site 3). The model performed well even during the non-growing season (last two image dates). Allen et al. 2007a used eight Landsat images acquired from April to September for comparing the METRIC model estimate with lysimeter measured ET and reported 30% averaged absolute differences for Sugar beet crop ($R^2 = 0.82$). When they omitted one image date of drying bare soil following precipitation, the average absolute difference was only 14%. There are many sources of uncertainties associated with comparison of EC tower-measured ET and model-estimated ET including model algorithm (model assumptions), tower observations (systematic and unsystematic bias), and scaling issues (flux footprint). Mu et al. (2009) has discussed in detail about these error sources. One of the most critical issues in the METRIC and the wMETRIC models is the selection of hot and cold pixels for anchoring the distribution of sensible and latent heat fluxes. Proper attention particularly to hot pixel ET_rF is necessary for high residual moisture content (Singh 2009; Singh and Irmak 2011) and vegetation amount (Choi et al. 2009).

Measured and estimated monthly evapotranspiration

Model-estimated daily ET values were used for computing monthly ET using cubic spline, fixed ET_rF, and linear

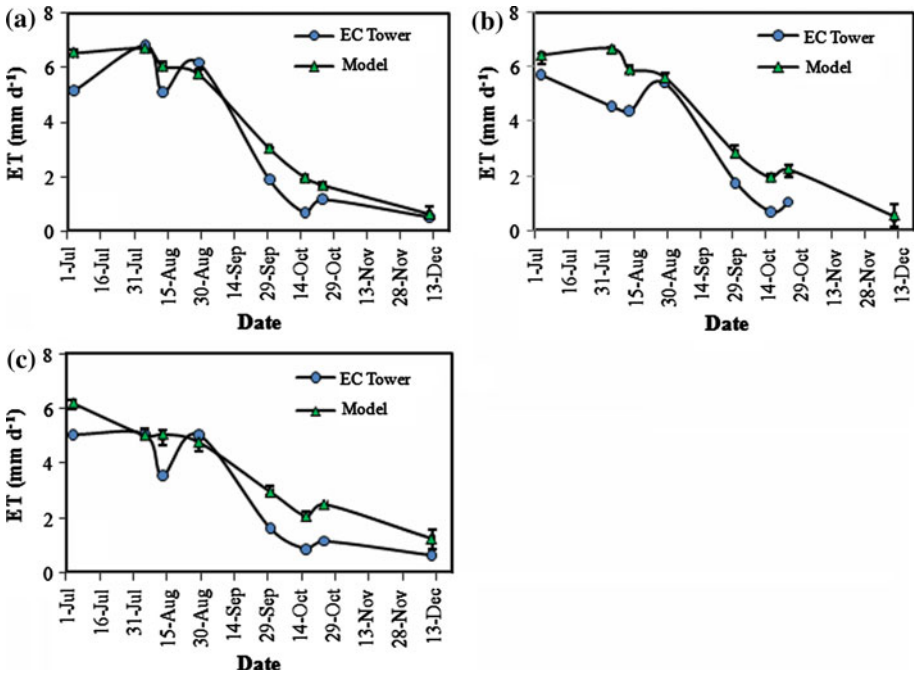

Fig. 4 Comparison of eddy covariance tower-measured daily evapotranspiration (*ET*) with model-estimated mean ET for (**a**) site 1, (**b**) site 2, and (**c**) site 3. The *error bars* with model-estimated ET show the range within 25 pixels (5 × 5) centered over the tower location

Table 3 Statistical details of comparison between eddy covariance tower-measured and model-estimated daily evapotranspiration at study sites

Site	Predictive error (%)	Standard error (mm day^{-1})	R^2 (−)
Site 1	17.7	0.7	0.93
Site 2	19.7	0.6	0.92
Site 3	30.2	0.6	0.89

methods. The computed monthly ET using cubic spline matched reasonably with EC tower-measured monthly ET during all months except October (Table 4). In fact all three methods poorly estimated monthly ET for October. This discrepancy for October is due to a couple of reasons. Though we used two images for the month of October, daily ET was overestimated on these 2 days at all three sites (Fig. 4). This overestimation propagated while computing monthly ET, resulting in large difference between measured and estimated values for October. Generally, the METRIC estimates for daily ET are randomly distributed (Allen et al. 2007a; Singh 2009), resulting in good estimate of seasonal ET due to compensation of under estimation on few dates with the overestimation on other dates. Another reason is the fact that maize at all three sites was harvested during this month (Table 1). During the maturity stage, most of the available energy is used for heating the atmosphere rather than transpiring the water. Once the crop is harvested, ET will reduce suddenly which is not captured by any of three methods for seasonal ET. Thereafter, monthly ET for November and December was nicely estimated even though no image was available for the month of November.

Statistical analysis has shown that estimated monthly ET was in reasonable agreement with the EC tower-measured monthly ET (Table 5). The results indicated that the variation between EC tower-measured and model-estimated mean monthly ET ranged from 17.8% (cubic spline at site 1) to 35.1% (fixed ET_rF at site 3). The standard error at site 1 and site 3 were similar but site 3 had higher predictive error due to low monthly ET value. The standard error ranged from 5 to 20 mm at all three sites, indicating good ability of these methods for computing monthly and seasonal ET. Allen et al. (2005) reported ±16% variations in monthly ET estimation as compared to lysimeter measurement at Montpelier, Idaho, using energy balance for July through October.

Seasonal evapotranspiration

The seasonal ET for 6 months (July through December, 2001) was computed using three methods for the study area. All three methods resulted in similar spatial distribution of seasonal ET (Fig. 5). As expected, seasonal ET was higher along the river network and lower in the built-up areas. Though visually these images appear to be similar, there are subtle differences in the seasonal ET values. The density plot of these images was plotted to explore the spatial differences among them (Fig. 6). There is some scattering along both sides of density plot for cubic spline and fixed ET_rF methods of seasonal ET, indicating some variation from point to point matching (Fig. 6a). But the

Table 4 Monthly evapotranspiration (mm) at three sites using eddy covariance (EC) tower and three different methods

		July	August	September	October	November	December
Site 1	EC tower	124	144	83	28	14	16
	Cubic spline	145	158	87	67	15	10
	Fixed	162	154	90	67	27	9
	Linear	162	156	89	67	25	8
Site 2	EC tower	123	126	69	24[a]	b	b
	Cubic spline	144	155	82	71	32	7
	Fixed	160	151	86	71	33	8
	Linear	159	153	85	70	30	7
Site 3	EC tower	111	117	70	28	16	15
	Cubic spline	121	129	77	76	42	17
	Fixed	144	124	80	76	42	18
	Linear	143	126	80	76	40	17

[a] Data for October are from October 1 to October 26

[b] No data were available for November and December months

Table 5 Statistical summary of monthly evapotranspiration (July–December) at three sites using fixed, linear, and cubic spline methods as compared to eddy covariance measurements

Site	Predictive error (%)			Standard error (mm)			R^2 (−)		
	Cubic spline	Fixed	Linear	Cubic spline	Fixed	Linear	Cubic spline	Fixed	Linear
Site 1	17.8	24.8	24.2	18	20	20	0.94	0.92	0.93
Site 2	19.7	24.7	24.7	5	10	8	0.99	0.97	0.98
Site 3	29.2	35.1	34.9	18	20	19	0.87	0.87	0.88

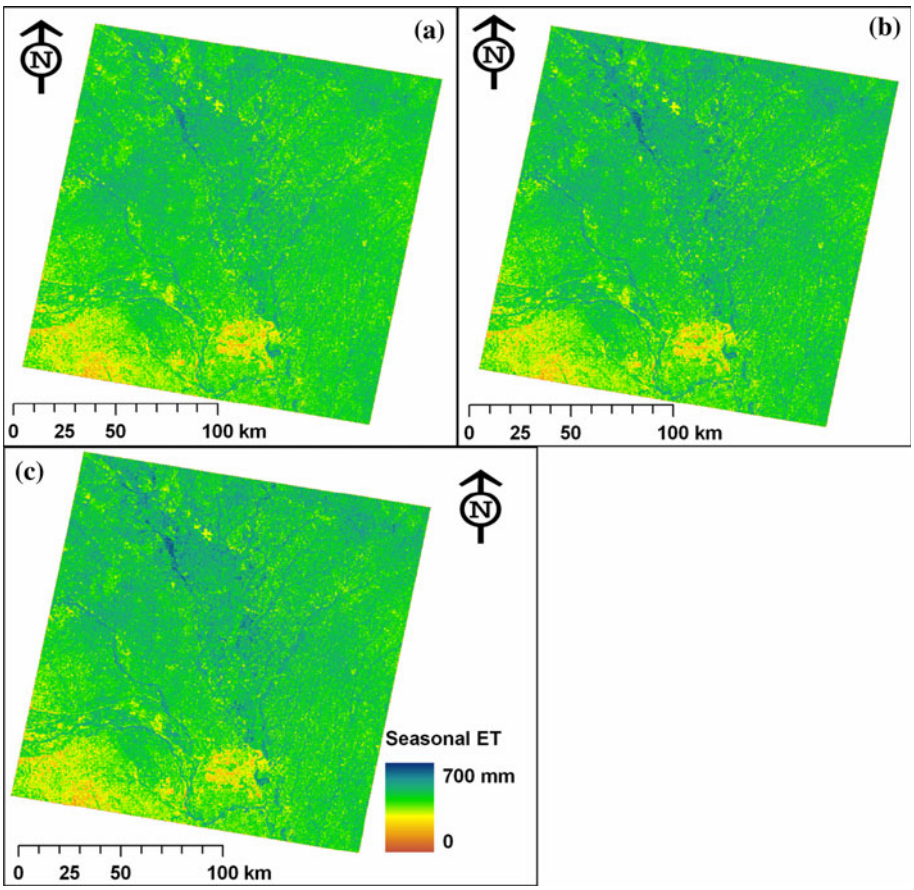

Fig. 5 Seasonal evapotranspiration (ET) (July 1 to December 31, 2001) map using (**a**) cubic spline, (**b**) fixed, and (**c**) linear method. The *same legend* can be used for all three images

majority of the pixels (high pixel density) were having similar seasonal ET distribution concentrated within the seasonal ET range of 300 mm to about 600 mm. Similar trend was also observed for density plot between cubic spline and linear method of seasonal ET (Fig. 6b). In comparison, a very narrow strip of density plot was observed between fixed ET_rF and linear methods, indicating similarities between these two methods of seasonal ET.

Validation of the seasonal ET maps was carried out using EC tower values (Fig. 7). It should be noted that most of the overestimation resulted from the overestimation during the month of October as discussed in the previous section. Our results indicated that there was no statistically significant difference ($P > 0.05$) at 95% confidence level among the cubic spline, fixed ET_rF, and linear methods for computing seasonal ET from temporal ET estimates. Overall, the cubic spline method resulted in the lowest standard error of 6 mm (1.67%) followed by fixed ET_rF (7 mm), and linear method (8 mm). Singh et al. (2008) reported seasonal ET using SEBAL model with linear interpolation of evaporative fraction within 5% of the Bowen ratio measured seasonal ET (May through October). Since Bowen ratio method assumes the closure of energy budget, it is possible that measured ET is in better agreement with model-estimated ET. Since the ET estimated on the days of satellite overpass are used in computing seasonal ET, it is important to have good estimate of daily ET. In comparison with ET estimates on the days of satellite overpass, the interpolation methods have less effect on estimated seasonal ET.

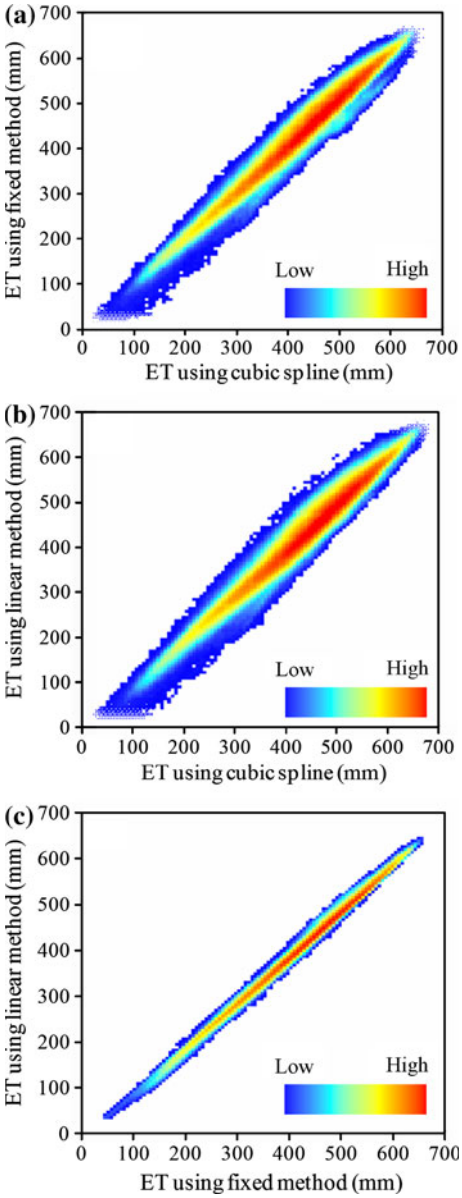

Fig. 6 Density plot of seasonal evapotranspiration (ET) image feature space for (**a**) cubic spline versus fixed method (**b**) cubic spline versus linear method, and (**c**) fixed versus linear method. The *color ramp* shows the relative pixel density

Conclusions

Seasonal ET over large area is important for water resources planning and management. Many modeling approaches in hydrology and ecology require spatial distribution of ET at resolution higher than daily time step. In this study, daily ET was estimated using eight Landsat images with the METRIC model in conjunction with the wMETRIC energy balance model. The model performed well in estimating daily ET while comparing with EC tower measurements with a standard error of less than 0.7 mm day^{-1}. Estimated daily ET on days of satellite acquisition was used to compute monthly and seasonal ET using cubic spline, fixed ET_rF, and linear methods. Statistical comparison of these three different methods for computing seasonal ET has shown that these three methods are statistically not significantly different. This was further

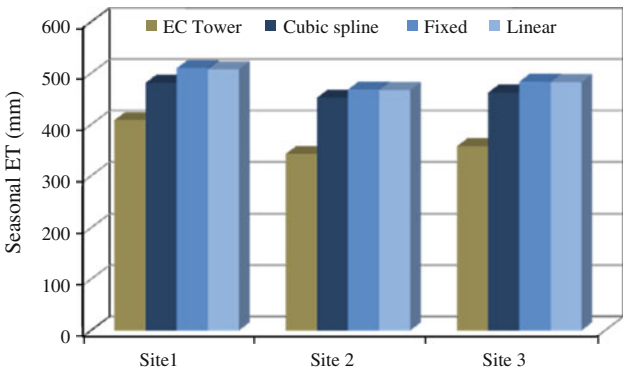

Fig. 7 Comparison of seasonal evapotranspiration (1st July to 31st December 2001) at site 1, site 2, and site 3 using EC tower, cubic spline, fixed, and linear methods. Seasonal ET values for site 2 are from July 1 to October 26, 2001

supported by the density plot of the spatial distribution of the seasonal ET. Majority of the pixels in one method of interpolation corresponded well with the other interpolation method. Among the three methods, cubic spline resulted in the lowest standard error. Further testing of this approach for multiple years is suggested to evaluate the inter-annual variation.

Acknowledgments This work was performed under USGS contract 08HQCN0007 with support from the Mendenhall Program of the US Geologic Survey through the Geographic Analysis and Mapping (GAM) and Land Remote Sensing (LRS) programs award to the Land Cover Applications and Global Change Project. We are thankful to our colleagues Jinxun Liu and Yiping Wu for reviewing the initial draft of this manuscript. Valuable comments from the two anonymous reviewers are greatly appreciated. The authors gratefully acknowledge the use of weather data from the High Plains Regional Climate Center, University of Nebraska-Lincoln. Any use of trade, product, or firm names is for descriptive purposes only and does not imply indorsement by the US Government.

Appendix: METRIC and wMETRIC models

A brief description of computational steps of Mapping Evapotranspiration at high Resolution with Internalized Calibration (METRIC) and the wet METRIC (wMETRIC) models is provided here. Readers interested in detailed process and procedures are advised to refer to Allen et al. (2007b, c) for the METRIC model and Singh and Irmak (2011) for the wMETRIC model. The computational processes are similar unless mentioned otherwise.

The net radiation (R_n) at the land surface is the difference of all the incoming and outgoing fluxes and computed as:

$$R_n = R_s\downarrow - \alpha R_s\downarrow + R_l\downarrow - R_l\uparrow - (1-\varepsilon_o)R_l\downarrow \quad (12)$$

where $R_s\downarrow$ is the incoming shortwave radiation (W m^{-2}), α is the surface albedo (unitless), $R_l\downarrow$ is the incoming longwave radiation (W m^{-2}), $R_l\uparrow$ is the outgoing longwave radiation (W m^{-2}) and ε_o is the surface thermal emissivity (unitless). $R_s\downarrow$ is computed as a constant for the time of satellite image acquisition under the clear sky condition as:

$$R_s\downarrow = G_{sc}\cos\theta\, d_r\, \tau_{sw} \quad (13)$$

where G_{sc} is the solar constant (W m^{-2}), θ is the solar incident angle (degree), d_r is the inverse square of the relative earth–sun distance in astronomical unit, and τ_{sw} is the broadband atmospheric transmissivity (unitless). $R_l\downarrow$ and $R_l\uparrow$ were computed as follows:

$$R_l\downarrow = \varepsilon_a\,\sigma\,T_a^4 \quad (14)$$

$$R_l\uparrow = \varepsilon_o\,\sigma\,T_s^4 \quad (15)$$

where ε_a is the effective atmospheric emissivity (unitless), σ is the Stefan-Boltzmann constant (W m^{-2} K^{-4}), T_a is the near surface air temperature (K), ε_o is the broadband surface emissivity (unitless), and T_s is the surface temperature (K).

Soil heat flux (G) was computed as follows:

$$G = [0.00647(T_s - 272.15) - 0.0955\text{NDVI} - 0.05]R_n \quad (16)$$

where NDVI is the normalized difference vegetation index (unitless).

Sensible heat flux (H) was estimated using the aerodynamic-based heat transfer equation as:

$$H = \frac{\rho_a C_p dT}{r_{ah}} \quad (17)$$

where ρ_a is the air density (kg m^{-3}), C_p is the specific heat of air at constant pressure (J kg^{-1} K^{-1}), dT is the temperature difference (K) between two heights z_1 (0.1 m) and z_2 (2 m), and r_{ah} is the aerodynamic resistance to heat transfer (s m^{-1}). The dT is computed for each pixel based on linear relation between dT and T_s for the anchor (hot and cold) pixels as

$$dT = aT_s + b \quad (18)$$

where a and b are the correlation coefficients for each satellite image based on reliable and accurate estimation of H at the anchor pixels. Since the stability of the atmosphere affects the aerodynamic resistance to heat transfer, stability correction was applied using Monin–Obukhov length parameter in an iterative process.

In the METRIC model, H at the cold pixel is computed based on corresponding R_n, G, and instantaneous alfalfa referenced ET (ET$_r$) values as follows:

$$H = R_n - G - 1.05\lambda\text{ET}_r \quad (19)$$

The H at the hot pixel in the METRIC model is computed based on alfalfa referenced ET fraction (ET$_r$F) for the dry soil surface from water balance model following FAO 56 (Allen et al. 1998) as:

$$H = R_n - G - \text{ET}_r\text{F}\ \lambda\text{ET}_r \quad (20)$$

In the wMETRIC model, H at the cold pixel was computed based on the Priestley–Taylor model (Priestley and Taylor 1972):

$$H = R_n - G - \alpha\frac{\Delta}{\Delta+\gamma}(R_n - G) \quad (21)$$

The H at the hot pixel in the wMETRIC model was computed as:

$$H = R_n - G - \text{ET}_r\text{F}\ \alpha\frac{\Delta}{\Delta+\gamma}(R_n - G) \quad (22)$$

Once the instantaneous R_n, G and H were determined, the instantaneous latent heat flux (LE, W m^{-2}) was estimated using equation:

$$\mathrm{LE} = R_\mathrm{n} - G - H \tag{23}$$

Based on the LE values, the instantaneous evapotranspiration ($\mathrm{ET_{ins}}$, mm $\mathrm{h^{-1}}$) was calculated as:

$$\mathrm{ET_{ins}} = 3,600\frac{\mathrm{LE}}{\lambda} \tag{24}$$

where λ is the latent heat of vaporization (J $\mathrm{kg^{-1}}$) and computed as

$$\lambda = [2.501 - 0.00236(T_s - 273)]10^6 \tag{25}$$

The reference ET fraction ($\mathrm{ET_rF}$) was computed based on $\mathrm{ET_{ins}}$ and alfalfa referenced ET ($\mathrm{ET_r}$, mm $\mathrm{h^{-1}}$) from the weather data as follows:

$$\mathrm{ETrF} = \frac{\mathrm{ET_{ins}}}{\mathrm{ET_r}} \tag{26}$$

Finally, the daily ET ($\mathrm{ET_{24}}$, mm $\mathrm{day^{-1}}$) at each pixel within the image was computed as:

$$\mathrm{ET_{24}} = \mathrm{ET_rF}\ \mathrm{ET_{r24}} \tag{27}$$

where $\mathrm{ET_{r24}}$ is the alfalfa referenced ET on daily basis (mm $\mathrm{day^{-1}}$) based on summed up hourly $\mathrm{ET_r}$.

References

Allen RG, Pereira LS, Raes D, Smith M (1998) Crop evapotranspiration: guidelines for computing crop water requirements. In: United Nations FAO, Irrigation and Drainage Paper 56. FAO, Rome

Allen RG, Tasumi M, Morse A, Trezza R (2005) A landsat-based energy balance and evapotranspiration model in Western US water rights regulation and planning. Irrig Drainage Syst 19:251–268

Allen RG, Tasumi M, Morse AT, Trezza R, Wright JL, Bastiaanssen W, Kramber W, Lorite I, Robison CW (2007a) Satellite-based energy balance for mapping evapotranspiration with internalized calibration (METRIC)-Applications. J Irrig Drain Eng 133(4):395–406

Allen RG, Tasumi M, Trezza R (2007b) Satellite-based energy balance for mapping evapotranspiration with internalized calibration (METRIC)–Model. J Irrig Drain Eng 133(4):380–394

Allen RG, Tasumi M, Trezza R (2007c) METRIC mapping evapotranspiration at high resolution applications manual for landsat satellite imagery version 2.0.2. University of Idaho, Kimberly

ASCE-EWRI (2005) The ASCE standardized reference evapotranspiration equation. Environmental and Water Resource Institute (EWRI) of the American Society of Civil Engineers (ASCE) Standardization of Reference Evapotranspiration Committee. ASCE, Reston, Virginia, p 216

Bastiaanssen WGM, Pelgrum H, Wang J, Ma Y, Moreno J, Roerink GJ, Van der Wal T (1998a) A remote sensing surface energy balance algorithm for land (SEBAL): 2 validation. J Hydrol 212–213:213–229

Bastiaanssen WGM, Menenti M, Feddes RA, Holtslag AAM (1998b) A remote sensing surface energy balance algorithm for land (SEBAL): 1 formulation. J Hydrol 212–213:198–212

Bastiaanssen WGM, Ahmad MD, Chemin Y (2002) Satellite surveillance of evaporative depletion across the Indus Basin. Water Resour Res 38(12):1273. doi:101029/2001WR000386

Beer C, Reichstein M, Cialis P, Farquhar GD, Papale D (2007) Mean annual GPP of Europe derived from its water balance. Geophys Res Lett 34:L05401. doi:101029/2006GL029006

Brutseart W, Sugita M (1992) Application of self-preservation in the diurnal evolution of the surface energy balance budget to determine daily evaporation. J Geophys Res 97(D17):18377–18382

Chavez JL, Neale CMU, Prueger JH, Kustas WP (2008a) Daily evapotranspiration estimates from extrapolating instantaneous airborne remote sensing ET values. Irrig Sci 27:67–81

Chavez JL, Gowda PH, Howell TA, Neale CMU, Copeland KS (2008b) Estimating seasonal ET from multispectral airborne imagery: an evaluation of interpolation-extrapolation techniques. ASABE annual international meeting, Providence, Rhode Island, paper no # 083637

Choi M, Kustas WP, Anderson MC, Allen RG, Li F, Kjaersgaard JH (2009) An intercomparison of three remote sensing-based surface energy balance algorithms over a corn and soybean production region (Iowa, US) during SMACEX. Agric Forest Meteorol 149:2082–2097

Gerald CF, Wheatley PO (2004) Applied numerical analysis, 7th edn. Pearson/Addison-Wesley, Boston

Gowda PH, Chavez JL, Colaizzi PD, Evett SR, Howell TA, Tolk JA (2008) ET mapping for agricultural water management: present status and challenges. Irrig Sci 26:223–237

Hollinger DY, Richardson AD (2005) Uncertainty in eddy covariance measurements and its application to physiological models. Tree Physiol 25:873–885

Moore CJ (1986) Frequency response correction for eddy correlation systems. Boundary-Layer Meteorol 37:17–35

Mu Q, Jones LA, Kimball JS, McDonald KC, Running SW (2009) Satellite assessment of land surface evapotranspiration for the pan-Arctic domain. Water Resour Res 45. doi:101029/2008WR007189

Nemani RK, White M, Thornton P, Nishida K, Reddy S, Jenkins J, Running S (2002) Recent trends in hydrologic balance have enhanced the terrestrial carbon sink in the United States. Geophys Res Lett 29(10):106-1–106-4. doi:101029/2002GL014867

Priestley CHB, Taylor RJ (1972) On the assessment of surface heat flux and evaporation using large-scale parameters. Mon Weather Rev 100:81–92

Shuttleworth WJ, Gurney RJ, Hsu AY, Ormsby JP (1989) FIFE: the variation in energy partitioning at surface flux sites. IAHS Red Book series no 186:67–74

Singh RK (2009) Geospatial approach for estimating land surface evapotranspiration. PhD dissertation, University of Nebraska

Singh RK, Irmak A (2011) Treatment of anchor pixels in METRIC model for improved estimation of sensible and latent heat fluxes. Hydrol Sci J (accepted)

Singh RK, Irmak A, Irmak S, Martin DL (2008) Application of SEBAL model for mapping evapotranspiration and estimating surface energy fluxes in south-central Nebraska. J Irrig Drain Eng 134(3):273–285

Suyker AE, Verma SB (2008) Interannual water vapor and energy exchange in an irrigated maize-based agroecosystem. Agril Forest Meteorol 148:417–427

Suyker AE, Verma SB (2009) Evapotranspiration of irrigated and rainfed maize-soybean cropping systems. Agril Forest Meteorol 149:443–452

Suyker AE, Verma SB (2010) Coupling of carbon dioxide and water vapor exchanges or irrigated and rainfed maize-soybean cropping systems and water productivity. Agril Forest Meteorol 150:553–563

Trezza R (2002) Evapotranspiration using a satellite-based surface energy balance with standardized ground control. PhD dissertation, Utah State University

Twine TE, Kustas WP, Norman JM, Cook DR, Houser PR, Meyers TP, Prueger JH, Starks PJ, Wesely ML (2000) Correcting eddy-covariance flux underestimates over a grassland. Agril Forest Meteorol 103:279–300

Verma SB, Dobermann A, Cassman KG, Walters DT, Knops JM, Arkebauer TJ, Suyker AE, Burba GG, Amos B, Yang H, Ginting D, Hubbard KG, Gitelson A, Water-Shea EA (2005) Annual carbon dioxide exchange in irrigated and rainfed maize-based agroecosystems. Agric For Meteorol 131:77–96

Webb EK, Pearman GI, Leuning R (1980) Correction of flux measurements for density effects due to heat and water vapor transfer. Q J Roy Meteorol Soc 106:85–100

Wilson KB, Baldocchi DD, Aubinet M, Berbigier P, Bernhofer C, Dolman H, Falge E, Field C, Goldstein A, Granier A, Grelle A, Halldor T, Hollinger D, Katul G, Law BE, Lindroth A, Meyers T, Moncrieff J, Monson R, Oechel W, Tenhunen J, Valentini R, Verma S, Vesala T, Wofsy S (2002) Energy partitioning between latent and sensible heat flux during the warm season at FLUXNET sites. Water Resource Res 38:1294–1305